Ocean Dynamics (2012) 62:1229–1243
DOI 10.1007/s10236-012-0556-2

Assessing the fidelity of surface currents from a coastal ocean model and HF radar using drifting buoys in the Middle Atlantic Bight

Liang Kuang · Alan F. Blumberg · Nickitas Georgas

Received: 20 September 2011 / Accepted: 29 May 2012 / Published online: 27 June 2012

Abstract The rapid expansion of urbanization along the world's coastal areas requires a more comprehensive and accurate understanding of the coastal ocean. Over the past several decades, numerical ocean circulation models have tried to provide such insight, based on our developing understanding of physical ocean processes. The systematic establishment of coastal ocean observation systems adopting cutting-edge technology, such as high frequency (HF) radar, satellite sensing, and gliders, has put such ocean model predictions to the test, by providing comprehensive observational datasets for the validation of numerical model forecasts. The New York Harbor Observing and Prediction System (NYHOPS) is a comprehensive system for understanding coastal ocean processes on the continental shelf waters of New York and New Jersey. To increase confidence in the system's ocean circulation predictions in that area, a detailed validation exercise was carried out using HF radar and Lagrangian drifter-derived surface currents from three drifters obtained between March and October 2010. During that period, the root mean square (RMS) differences of both the east–west and north–south currents between NYHOPS and HF radar were approximately 15 cm s^{-1}. Harmonic analysis of NYHOPS and HF radar surface currents shows similar tidal ellipse parameters for the dominant M_2 tide, with a mean difference of 2.4 cm s^{-1} in the semi-major axis and 1.4 cm s^{-1} in the semi-minor axis and 3° in orientation and 10° in phase. Surface currents derived independently from drifters along their trajectories showed that NYHOPS and HF radar yielded similarly accurate results. RMS errors when compared to currents derived along the trajectory of the three drifters were approximately 10 cm s^{-1}. Overall, the analysis suggests that NYHOPS and HF radar had similar skill in estimating the currents over the continental shelf waters of the Middle Atlantic Bight during this time period. An ensemble-based set of particle tracking simulations using one drifter which was tracked for 11 days showed that the ensemble mean separation generally increases with time in a linear fashion. The separation distance is not dominated by high frequency or short spatial scale wavelengths suggesting that both the NYHOPS and HF radar currents are representing tidal and inertial time scales correctly and resolving some of the smaller scale eddies. The growing ensemble mean separation distance is dominated by errors in the mean flow causing the drifters to slowly diverge from their observed positions. The separation distance for both HF radar and NYHOPS stays below 30 km after 5 days, and the two technologies have similar tracking skill at the 95 % level. For comparison, the ensemble mean distance of a drifter from its initial release location (persistence assumption) is estimated to be greater than 70 km in 5 days.

Keywords HF radar · NYHOPS · GNOME · Coastal circulation model · Drifter · Drifter-derived currents · Model validation · Model skill · Particle tracking

Responsible Editor: Michel Olagnon

This article is part of the Topical Collection on *Advances in Search and Rescue at Sea*

L. Kuang · A. F. Blumberg (✉) · N. Georgas
Center for Maritime Systems, Stevens Institute of Technology,
Castle Point on Hudson,
Hoboken, NJ 07030, USA
e-mail: ablumberg@stevens.edu

1 Introduction

The modern world is experiencing the greatest human migration in history. The inland rural population is moving to the coast. Now over 50 % of the world's population lives in

coastal areas. In the USA alone, the figure is 80 % (U.S. National Academies 2010). In the largest coastal cities, the 136 port cities around the world that have more than one million inhabitants, there is a population of 400 million people. These urban coastal areas are especially susceptible to disruption from extremes of weather, tectonic forces, and human activity. Having an accurate knowledge of the currents that are found in coastal regions is important for various applications, such as search and rescue operations, coastal ecosystem management (e.g., tracking fish larvae and dispersal of pollutants; Fan et al. 2004; North et al. 2010), and tidal energy quantification and harvesting. Various ocean technologies, including satellite and other remote imaging (Dugan and Piotrowski 2003), high frequency radar (HF radar, Kohut et al. 2006; Parks et al. 2009; Roarty et al. 2010; Gurgel et al. 2011), satellite-tracked drifters (Fratantoni 2001; Poulain 2001), gliders (Rudnick et al. 2004), unmanned underwater vehicles, etc., have been deployed by oceanographers and meteorologists, to improve understanding of the ocean dynamics. Coastal ocean models have also come into their own right, predicting currents and other ocean constituents with considerable skill (e.g., Samelson et al. 2008; Georgas and Blumberg 2010; Gopalakrishnan and Blumberg 2012).

The Middle Atlantic Bight (MAB) is the part of the United States East Coast continental shelf that runs from Cape Cod, Massachusetts to Cape Hatteras, North Carolina. Its coastline is one of the most populous regions in the world. The understanding of currents and circulation in the MAB is of critical importance to the economic and social development in this region. The general circulation pattern has been studied extensively and is well understood. In general, the MAB has water characteristics that are typically lower in temperature and salinity than the adjacent offshore slope water (Brian 2009). Chang et al. (2002) showed that the general circulation in the MAB originates with the mixing of the Gulf of Maine and Scotian Shelf waters to the north as modified by local processes (seasonal heating, cooling, precipitation, and evaporation). This water flows southward over and around Georges Bank and proceeds past Cape Cod into the MAB region (Brian 2009). Physical processes associated with river/estuary systems, coastal bathymetry, and the shelf slope interact with this water mass within the MAB region. The water does not exit the MAB at the shelf break but rather runs along the shelf and exits to the south near Cape Hatteras (Brian 2009). Studies by Rasmussen et al. (2005) showed that the cross shelf transport at the shelf-slope edge (shelf break) is small and supports the notion of large along-shelf transport in the MAB. Between 75 and 90 % of the along-shelf sub-inertial current energy can be attributed to wind-forced motions and freely propagating waves (Noble et al. 1983).

Currents in the MAB are influenced by many processes, including tides, winds, river flows, and coastal and shelf break upwelling and downwelling. Energetic tidal currents have been identified along the US east coast shelf. The M_2 tide is the dominant constituent and accounts for 80 % of tide energy in the central MAB. Spatial variability of the tidal currents between the Lower Hudson River and the Delaware Bay is found (Brian 2009). In the MAB, the subtidal flow along shelf is largely driven by winds and propagating free waves (Schulz et al. 2012). On the shelf break, there exists a cross-shelf geostrophic balance associated with a persistent along-shore jet that flows to the southwest (Flagg 1977). The Gulf Stream (Beardsley and Boicourt 1981) also affects the shelf break and outer shelf regions.

The development of land-based HF radar systems over the last several decades has provided a unique ocean observation platform capable of measuring near-surface ocean currents remotely from the shoreline. The HF radar system works on the principle of radio wave backscatter by ocean surface gravity waves in the frequency band 3–30 MHz and is capable of mapping ocean surface currents (~1 m deep) over a synoptic scale of the O (200 km) depending upon the transmitting frequency (Barrick et al. 1977; Paduan and Rosenfeld 1996; Paduan and Graber 1997; Graber et al. 1997). A HF radar network has been deployed for the MAB which provides shelf-wide realizations of surface currents every hour (Roarty et al. 2010). This HF radar observation system consists of more than 20 long-range stations, with locations all along the coast of the Middle Atlantic States.

At the same time, there exists a high fidelity coastal ocean forecast model of the same waters (Georgas and Blumberg 2010). The model is part of the New York Harbor Observing and Prediction System (NYHOPS), providing high spatial resolution predictions of water level, 3D circulation fields (currents, temperature, salinity, density, speed of sound), significant wave height, and period that are archived on an hourly basis for the coastal waters of New Jersey and New York.

In the present study, satellite-tracked drifters (Davis 1985) are used to validate the performance of both HF radar and NYHOPS from both Eulerian and Lagrangian perspectives in the MAB. The region is of interest for its importance as an urban coast and for being a highly productive biological zone. Here, we first comprehensively compare estimates of surface currents over the continental shelf portion of the MAB from the HF radar network data and the NYHOPS model predictions. Then, currents are determined from drifter locations over time along their trajectory and then compared to currents from the HF radar system and NYHOPS. And finally, particle-tracking-based simulations of drifter trajectories based on both the currents from the HF radar network and NYHOPS are compared to the observed drifter paths. Questions on the limit of useful trajectory predictions are then addressed. Limitations in both technologies (climatological

boundary condition for NYHOPS and HF radar signal coverage) during the period of this study are also presented.

2 Methods

2.1 Data and models

In the present work, three realizations of surface currents from NYHOPS, HF radar, and drifters have been used for comparison purposes. Each will be briefly described.

The HF radar deployed in the MAB is a long-range CODAR system which transmits electromagnetic waves at frequency of 5 MHz. The backscattered EM waves are analyzed using the CODAR Multiple Signal Classification (MUSIC) algorithm to derive hourly total currents at a depth of 1 m for the covered ocean. The HF radar currents used here cover the continental shelf portion of the MAB (Fig. 1). A total of 64 days HF radar data in alignment with the following drifter track date range were obtained. The HF radar total current vectors were computed at locations coincident to the NYHOPS model grid by combining the individual radials of 16 available HF radar stations (Fig. 1) in the MAB network using a temporal and spatial interpolation algorithm (Lipa and Barrick 1983). Radials were available, and total current vectors were computed, at hourly interval.

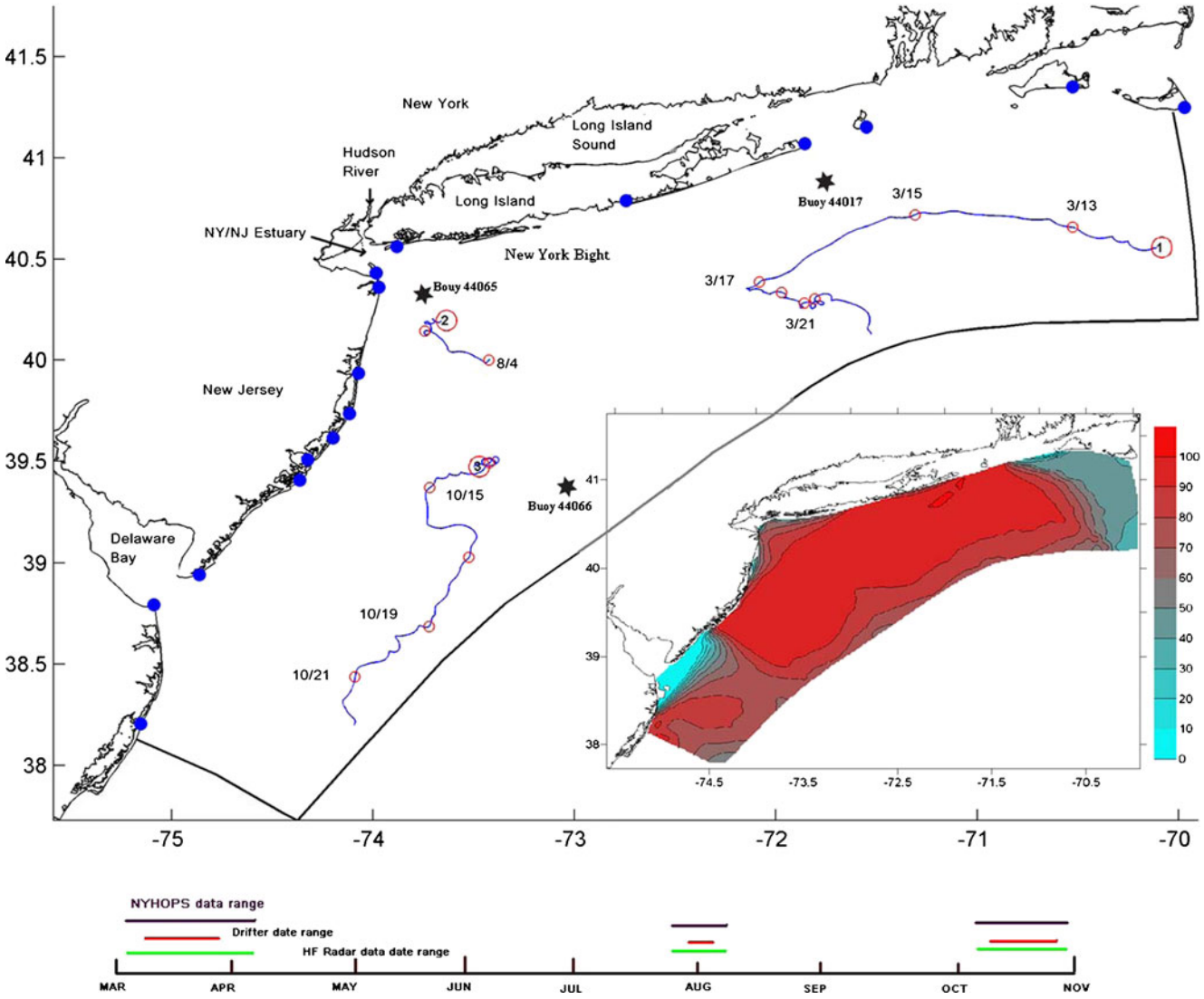

Fig. 1 Location map showing study domain. *Black lines* are for the coastline and open boundary of NYHOPS. *Blue lines* are the SLMDB drifter data available in year 2010 (three drifters with minimum time duration of 3 days inside the present study domain); *red dots* (and associated dates) show drifter positions every 2 days to illustrate drifter speed. *Blue dots* are locations of HF radar network stations. *Red numbered circles* represent initial release locations for each drifter. *Lower right insert* shows the spatial coverage map of HF radar data during the study period: *dark red* represents near 100 % coverage while *light cyan* shows near 0 % coverage. The *bottom insert* shows the illustration of time range of available data of the three different technologies. The *black stars* represent the three buoys that provide wind speed data used in this paper

The spatial and temporal coverage of the combined HF radar network varies in time, creating some gaps in the total vector retrievals. Coverage within the study domain was best away from the coast. It was also relatively low in the northern and southern parts of the MAB region and in the region next to the continental shelf break.

The specific type of drifter used here is called the self-locating marker datum buoy (SLMDB). It transmits its location via the ARGOS satellite every 30 min. This type of drifter buoy is designed to stay in the ocean surface, follow the near-surface currents at a depth of 1 m, and have minimal windage effects (Davis 1985). A clear picture of the ocean flow patterns from a Lagrangian perspective is thus obtained in near real time.

NYHOPS is a 3D operational forecast model for the New York/New Jersey Harbor Estuary and surrounding waters (Bruno et al. 2006; Georgas et al. 2009; Georgas 2010). The extent of the NYHOPS computational domain covering the MAB is shown in Fig. 1. The domain is discretized on an Arakawa "C" finite-difference grid with 147×452 cells, 15,068 of which are designated as water, with a horizontal resolution varying from 25 m (estuary) to 7.5 km (outer shelf). The depth of this region varies from 2 to 200 m at the shelf break where the NYHOPS open boundary is located. NYHOPS is forced at the open ocean lateral boundaries by total water level, waves, climatological temperature and salinity; It is also forced internally with thermodynamic inputs from river, stream, water pollution control plant discharges, and thermal power plant intakes/outfalls. Spatially variable surface boundary conditions for wind and heating and cooling are included. Quadratic friction is applied at the bottom based on internally calculated friction coefficients that include wave boundary layer effects (Grant and Madsen 1979; Georgas et al. 2007; Georgas 2010) and at the free surface through assimilation of surface ice cover friction (Georgas 2012). Several comprehensive skill assessment studies have been carried out (Fan et al. 2006; Georgas et al. 2007; Bhushan et al. 2009; Georgas and Blumberg 2008, 2010; DiLiberto et al. 2011). Currents at depths of 1–5 m (depending on the depth of the surface-most sigma layer in the model) computed by NYHOPS during calendar year 2010 were retrieved from archived data and used in this study.

2.2 Estimation of surface currents from drifters

Three drifter releases in the MAB in 2010 were used for the present study to assess current predictions. They all had a minimum ocean life of at least 4 days and were located in the NYHOPS domain away from its open boundaries. The drifter trajectories are shown in Fig. 1. Table 1 provides the drifter number, time, and position of first recording for each of the three drifters used in the analysis. The table also provides the total number of days the observed drifters were tracked. Drifter 2 was released near the mouth of the NY/NJ Estuary; it experienced currents typical of the Hudson River outflow plume (Chant et al. 2008). The other two drifters were deployed farther offshore where the currents were much stronger. The near-surface currents (at a depth of 0.5 m) derived from the locations of the drifters along their trajectory were used for assessing the skill of the HF radar system and NYHOPS for predicting sea-surface currents. Near-surface current components were calculated as in:

Table 1 Deployment history of the SLDMB drifters used in this study

Track no.	Start time	End time	Duration (days)
1	March 11, 2010	March 25, 2010	14
2	July 31, 2010	August 4, 2010	4
3	October 11, 2010	October 22, 2010	11

$$u(t_0) = \frac{x(t_1) - x(t_0)}{t_1 - t_0}$$
$$v(t_0) = \frac{y(t_1) - y(t_0)}{t_1 - t_0} \quad (1)$$

where, $[x(t_0), y(t_0)]$ is the location of drifter at time t_0, $[x(t_1), y(t_1)]$ is the location of drifter at the next time t_1, and $[u(t_0), v(t_0)]$ are the surface current components thus derived. For easier comparison to the collocated NYHOPS and HF radar current vectors, the derived surface current vectors from Eq. (1) were mapped on the same NYHOPS grid using the local approach (Fan et al. 2004), where the computed drifter current was assigned at the center of the nearest model grid box.

2.3 Assessment metrics

Three metrics are used here for determining the goodness of fit between the two technologies for deducing the surface currents and the drifter-based currents. They are the mean, the mean vector velocity difference (MVVD), and the root mean square difference (RMSD). The MVVD is defined as:

$$\mathrm{MVVD} = \sqrt{(\overline{u_1} - \overline{u_2})^2 + (\overline{v_1} - \overline{v_2})^2} \quad (2)$$

where $[\overline{u_i}, \overline{v_i}]$ (i=1, 2) are the mean of the east–west, north–south component of the surface current, respectively, from two different technologies.

In order to compare the performance of NYHOPS relative to the HF radar currents, the RMSD is defined as

$$\mathrm{RMSD}(x_i, y_j) = \sqrt{\frac{1}{T}\sum_{\tau=1}^{T}\left[M(t_\tau, x_i, y_j) - O(t_\tau, x_i, y_j)\right]^2} \quad (3)$$

where T is the number of comparison times, (x_i, y_j) is the grid

point of the model, and $M(t_\tau, x_i, y_j)$, $O(t_\tau, x_i, y_j)$ represent modeled value and observed value, respectively. The RMSD between hourly modeled and observed currents is computed at every model grid point with collocated HF radar retrievals (at 3,562 points). The spatially averaged RMSD of the sea-surface current is then computed to get an overall performance metric for predicting that parameter. A period of 64 days in 2010 that included the drifter deployments was considered.

Continuous surface current time series from NYHOPS and HF radar, between March 5, 2010 and April 10, 2010, were used to calculate the tidal amplitude, phase, and current ellipse parameters based on the least-squares harmonic analysis following T_tide by Pawlowicz Rich et al. (2002). Results were compared to observed tidal ellipses from historic current meter data collected in the MAB, tabulated in Moody et al. (1984). This was done to evaluate the ability of each technology to simulate the tidal signal.

2.4 Lagrangian particle tracking

Lagrangian particle tracking models have been created and used in search and rescue planning, predicting distributions of fish larvae, and oil spill fate and transport. With this in mind, assessing the skill of a set of currents in combination with a Lagrangian particle tracking model is very useful and complementary. Here, surface current fields derived by NYHOPS and HF radar are put to the test of reproducing observed Lagrangian trajectories with the use of a particle tracking model. Numerical particles are released at the same initial location and starting time as the observed drifters; their trajectories are then simulated. The separation distance between simulated and observed drifters is analyzed as a metric for assessing estimator performance. In this study, drifter 3 (Fig. 1) is used for the particle tracking analysis given the fact that the data coverage in that region is comparatively better, and currents from both NYHOPS and HF radar are for the most part reasonable, as explained in Section 3.2.

The particle tracking model used in this study is the General NOAA Operational Modeling Environment (GNOME), which is based on a Lagrangian particle tracking algorithm (Beegle-Krause 2001 expressed as:

$$x = x_0 + \int_{t_0}^{t_1} u(x,y,t)\mathrm{d}t + R_{(0,1)}\sqrt{6D(t_1 - t_0)} \quad (4)$$

$$y = y_0 + \int_{t_0}^{t_1} v(x,y,t)\mathrm{d}t + R_{(0,1)}\sqrt{6D(t_1 - t_0)} \quad (5)$$

where $[x, y]$ is the location of a particle at time t_1 that has experienced advection by a spatially and temporally varying surface current field $[u(x,y,t), v(x,y,t)]$ from its initial position of $[x_0, y_0;$ at time $t_0]$ and has been allowed to diffuse based on a constant isotropic horizontal diffusivity D with a square distribution. $R_{(0,1)}$ is the random number generator used in simulating diffusion as a random walk process. The locations of the particles in the GNOME simulations herein are thus updated by two processes: deterministic advection by ocean currents and random diffusion averaged in an ensemble fashion. GNOME has been widely used in rapid response to environmental hazard events, such as oil and chemical spills, and in search and rescue episodes. The code is available at http://response.restoration.noaa.gov/book_shelf/718_GNOMESetup.exe.

Following the methodology developed by Ullman et al. (2006) for simulating drifters in the MAB, 1,000 numerical particles were released and were allowed to move with currents based on the input current field and diffuse based on a uniform diffusion coefficient, D, of 100 m^2 s^{-1}. A sensitivity study of the diffusion coefficient was first performed that involved decreasing and increasing the coefficient by an order of magnitude. The results were that the separation distance between the simulated and real drifter in both cases was indeed much larger than that using 100 m^2 s^{-1}. Due to the negligible lee-way of wind effects on SLMDB drifters (Davis 1985), no windage forcing was used in GNOME simulation for both NYHOPS and HF radar particle tracking predictions. The trajectory of drifter 3 was divided into daily release points ("reseeding points"). Five-day GNOME runs were initiated by releasing the particles at each reseeding point, saving the locations of the position hourly. Eight such runs were considered and factored in an ensemble analysis. The accuracy of the drifter trajectory prediction was measured here by the ensemble mean separation distance between the real drifter and the simulated one. That distance was put into perspective by considering the persistence error, that is, the ensemble mean separation distance if one were to assume that each reseeded drifter remained at its release location (Ullman et al. 2006). If the separation distance is less than the persistence error, then the technology (NYHOPS or HF radar) is qualitatively able to reproduce longer term mean flows.

3 Results

3.1 Comparison between currents from NYHOPS and HF radar

Figure 2a shows the time-averaged surface flow in the MAB as measured by the HF radar technology (panel A) and as predicted by the NYHOPS model (panel B). The dates when the HF radar, NYHOPS, and drifters are available are shown in the timeline insert of Fig. 1. There are 64 days of hourly HF radar available between March and October 2010 for this study. Only areas that were sampled at least 50 % of the

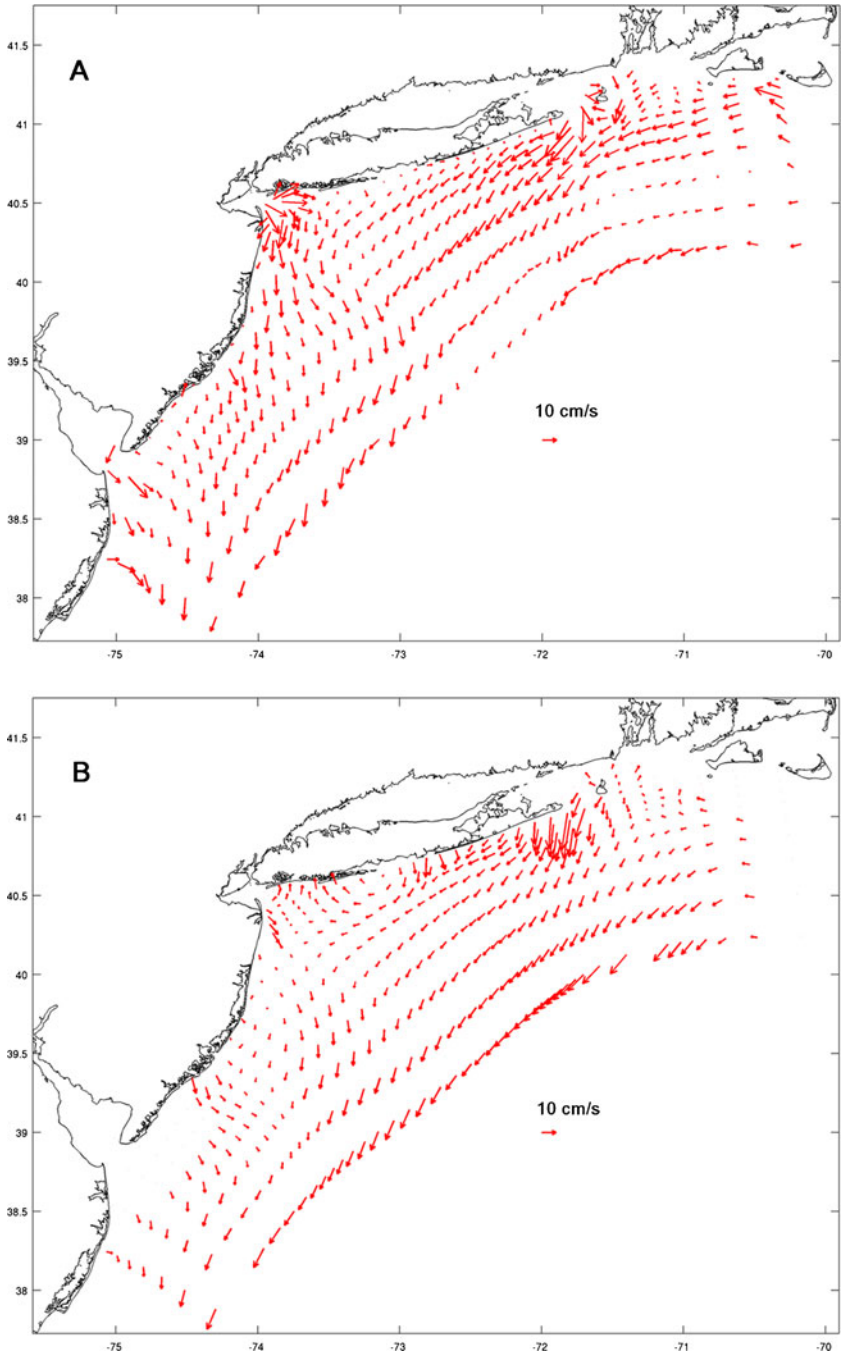

Fig. 2 **a** Vector plot of mean surface currents for NYHOPS (*A*) and HF radar (*B*) between March 4, 2010 and October 22. 2010 (the available dates used for the average are shown in the timeline insert of Fig. 1). Vector reference scale is 10 cm s^{-1} as shown. **b** Comparison of M_2 tidal ellipses in Middle Atlantic Bight between NYHOPS (*upper panel*)/HF (*lower panel*) radar and current meter observations (*red, thin line*)

time by the HF radar network during that time period (50 % coverage in the insert of Fig. 1) are used here to create meaningful longer term comparisons.

The mean vector currents plotted in Fig. 2a have much in common. They both have the correct mean flow pattern. This mean flow is well known, based on hydrography, drifters, shipboard current profiles, and moored current observations (see Beardsley and Boicourt 1981 for an early summary; also Lentz 2008a, b) as well as numerical modeling over many years (Blumberg and Galperin 1990; Xu and Oey 2011). The mean surface flow is 2 to 12 cm s^{-1} directed southward on the shelf and offshore. The currents are smallest at the inner shelf and largest at the shelf break (Gong et al. 2010).

Both the HF radar and NYHOPS currents show strong currents flowing out of the eastern end of Long Island Sound

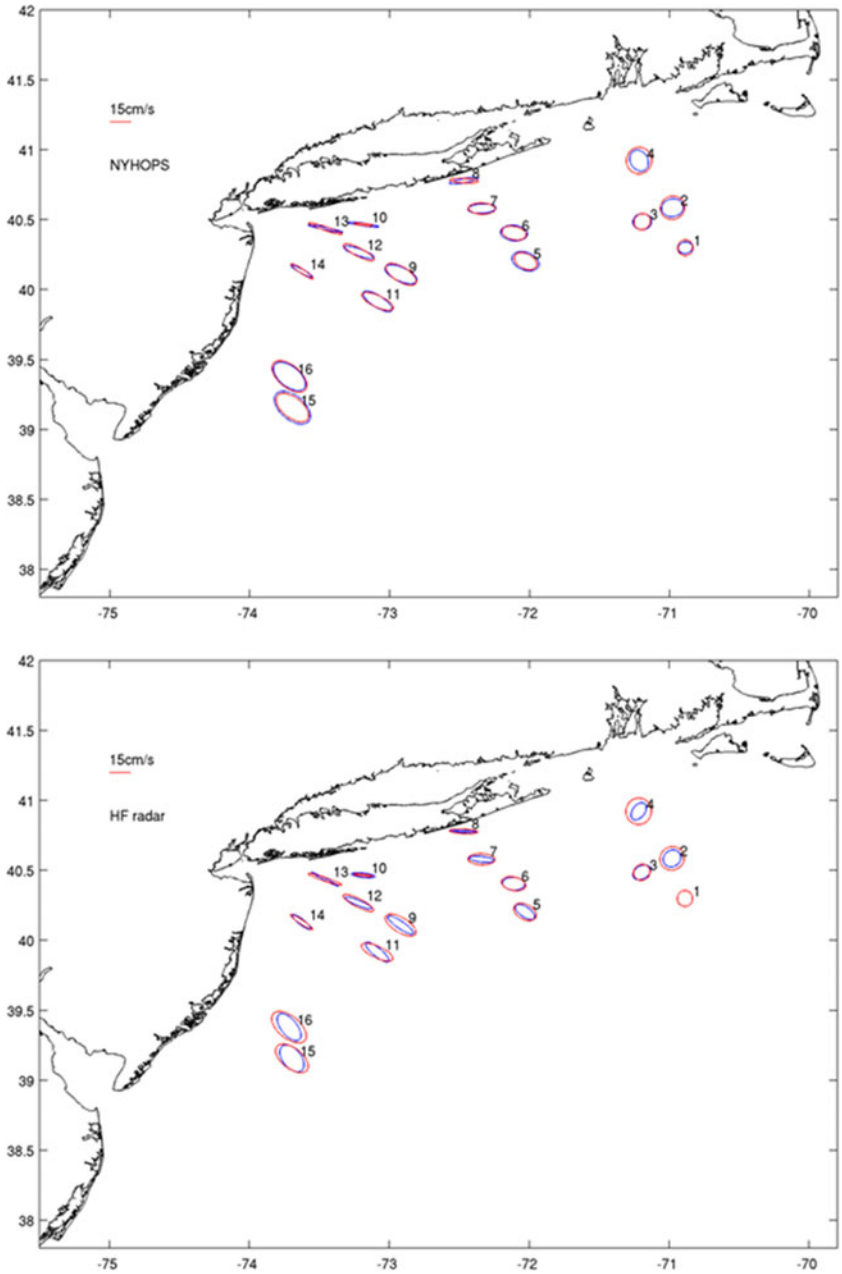

Fig. 2 continued.

in agreement with the currents observations of Gay et al. (2004). Only NYHOPS currents show the well-known flow exiting the NY/NJ Estuary (e.g., Chant et al. 2008). These are similar to those currents determined by Gong et al. (2010).

Calculated tidal ellipses are presented in Fig. 2b. The tidal ellipses are all traced clockwise in time and are generally oriented normal to isobaths (Moody et al. 1984). The tidal ellipses for NYHOPS and HF radar both exhibit the considerable observed spatial variability in amplitude and phase. Figure 2b (upper panel) shows that the tidal ellipses of NYHOPS agree well with observations for all 16 sites. HF radar-derived tidal ellipses are also similar. The difference between the HF radar and observed tidal ellipses is slightly larger at five sites (2, 4, 11, 15, and 16, Fig. 2b). The averaged misfits between observation and NYHOPS are 0.80 cm s^{-1} for semi-major axis and 0.38 cm s^{-1} for semi-minor axis and 18° in orientation and 25° in phase. The averaged misfits between observation and HF radar are 2.4 cm s^{-1} for semi-major axis and 1.4 cm s^{-1} for semi-minor axis and 22° in orientation and 35° in phase. The average difference between NYHOPS and HF radar is 1.6 cm s^{-1} for the semi-major axis and 1.1 cm s^{-1} for the semi-minor axis and 3° for orientation and 10° for

phase. It is apparent that NYHOPS and HF radar capture tidal currents correctly.

Contour maps of the RMS difference of the east–west and north–south components of the total (tidal and non-tidal) surface current between NYHOPS and HF radar are shown in Fig. 3. There are relatively large RMS differences at the entrance to the NY/NJ Estuary, near Long Island Sound, the entrance to Delaware Bay, and in the northeast portion of the MAB. The RMS difference contour map of the north–south component shows that the RMS difference is also large along the New Jersey coast, where the Hudson River fresh water plume exits the NY/NJ Estuary into the continental shelf.

The RMS difference for both the east–west and north–south components of the total surface currents between NYHOPS and HF radar is on the order of 15 cm s^{-1} for the majority of the MAB shelf region (Fig. 3). The RMS differences are as high as 50 cm s^{-1} in those areas where surface currents are usually strong, as in Delaware Bay, NY/NJ Estuary, Long Island Sound (Brian 2009; Chant et al. 2008). The normalized RMS difference of the east–west and north–south components of the surface currents between NYHOPS and HF radar by the maximal surface current has a value of 20 %. The normalized RMS difference of the east–west and north–south surface current components has similar distribution as the RMS difference (not shown). The

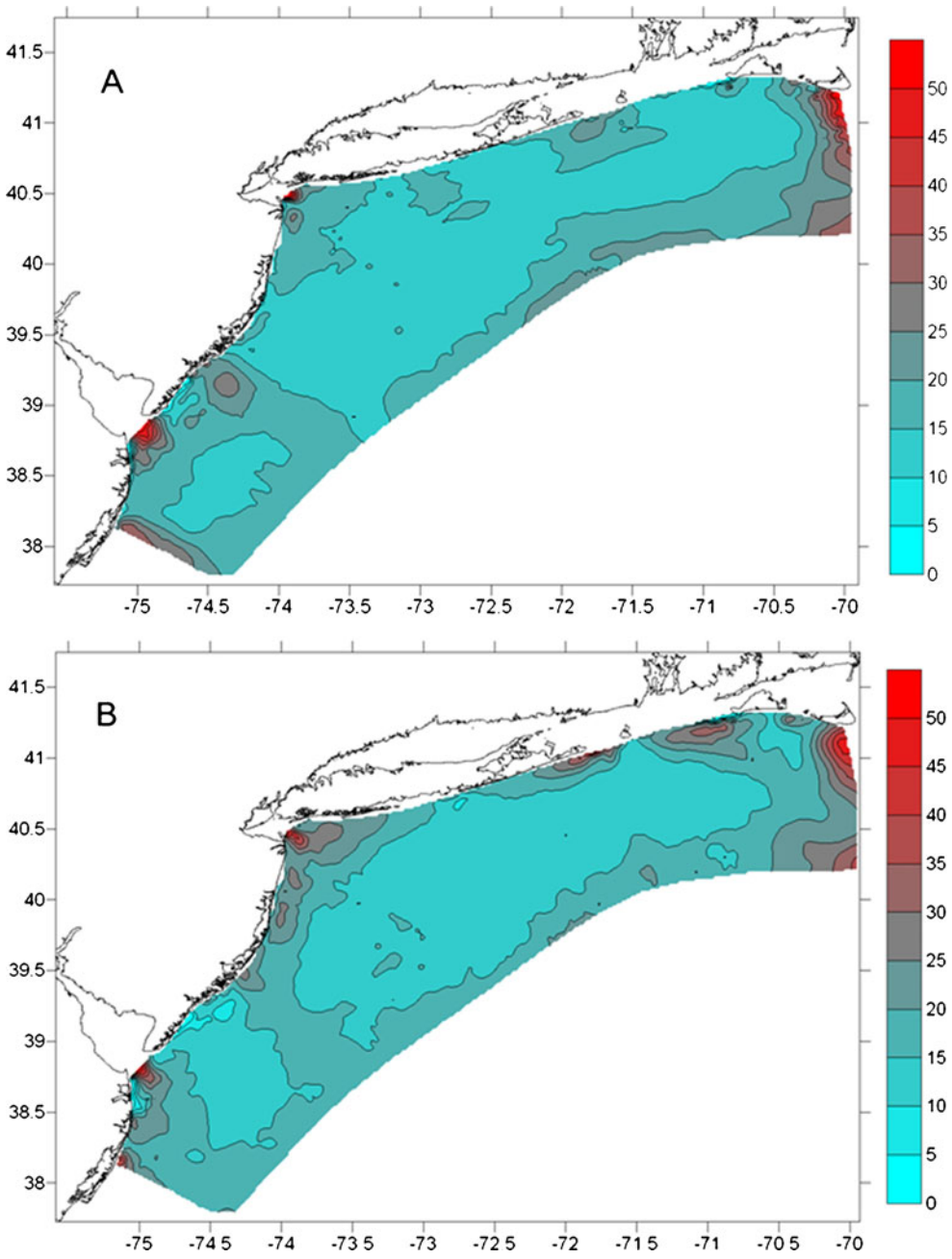

Fig. 3 Time-averaged root mean square difference (RMSD) contours of east–west (**a**) and north–south (**b**) surface currents between NYHOPS and HF radar inside the study domain using data at available dates shown in the timeline insert of Fig. 1. RMSD contour scale in centimeter per second

normalized RMS differences are as high as 90 % in those areas with stronger surface currents. The spatially averaged ratio of the RMS difference to the standard deviation of the HF radar currents is 1.5 for both the east–west and north–south components of the surface currents. If the two datasets were in best agreement, one would expect this ratio to be less than unity. The RMS difference of the non-tidal currents between NYHOPS and HF radar is on the order of 12 cm s^{-1} for the majority of the MAB shelf region (not shown). This analysis implies that the difference between NYHOPS and HF radar is mostly from the non-tidal effects, due to meteorology, buoyant plumes common in the MAB and the influences of the offshore ocean. The difference of the representative depth of each technology is one factor that contributes to the differences between NYHOPS (the first sigma layer depth varies from 1 to 5 m) and HF radar (1 m depth). Consideration of surface shear and Ekman layer can also play a role in the discrepancies. Also, the quality of HF radar signal and its temporal/spatial coverage plays a big role in the accuracy of HF radar observation.

3.2 Comparison of surface currents—NYHOPS, HF radar, and drifters

Time series of surface currents along the three drifter trajectories are shown in Figs. 4, 5, and 6. Record discontinuities in these figures are due to gaps in the HF radar retrievals. Differences between the NYHOPS and HF radar surface current vs. the drifter-based currents are also included. Tables 2 and 3 summarize the comparisons of these surface current estimators with regard to the mean, MVVD, and RMS difference metrics.

Drifter 1 was in the water for 14 days during March 2010. It was deployed in the northeastern portion of the shelf. It appears from Fig. 4 that both NYHOPS and HF radar are able to reproduce the currents over much of the period. HF radar retrievals were especially good during March 15 to 17 when there was a strong flow to the south due to sustained winds blowing from the northwest at over 10 m s^{-1}. However, the difference between HF radar/NYHOPS and drifter is bigger at times when the wind is strong (Fig. 4). The

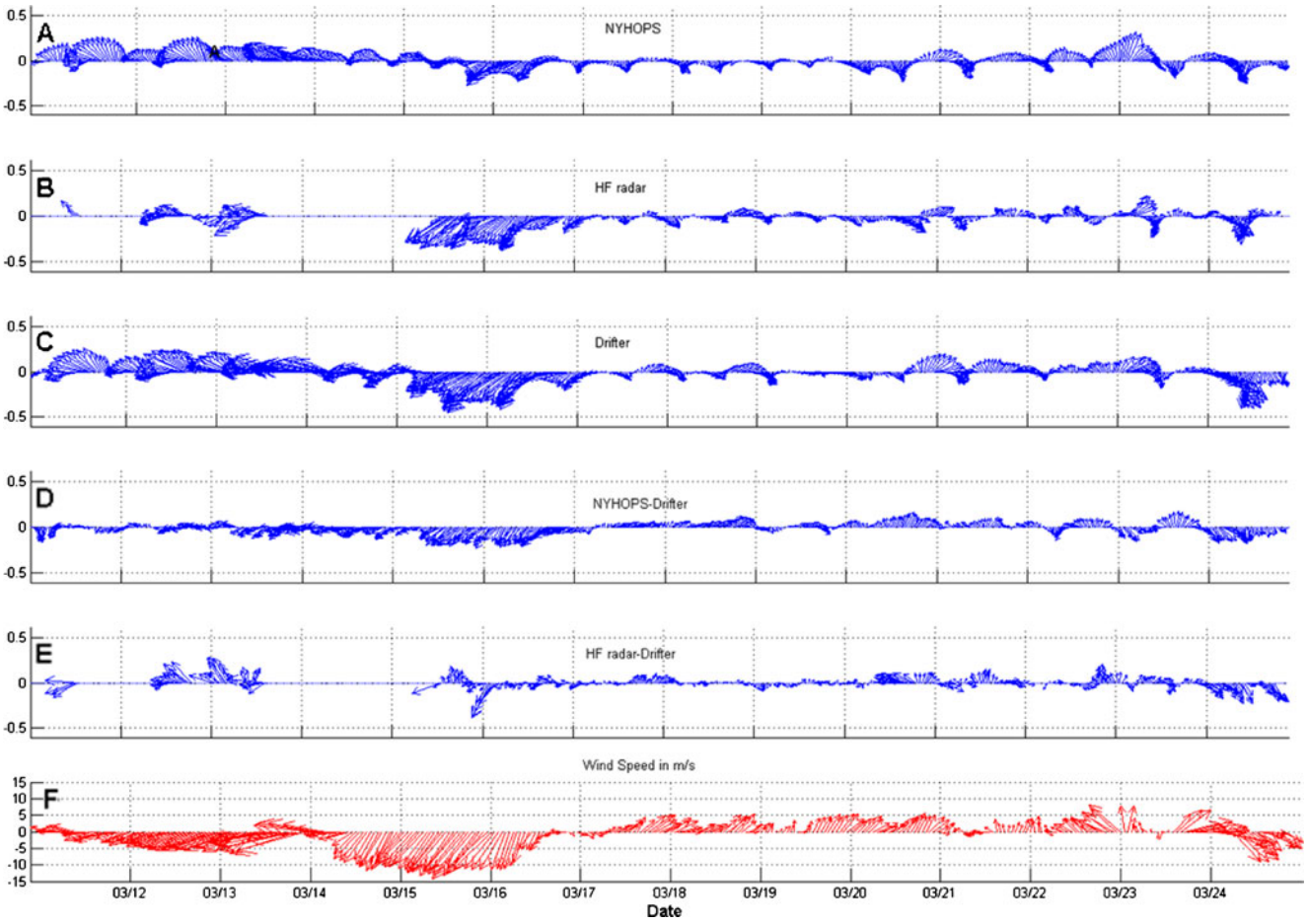

Fig. 4 Vector plots of surface current along track 1 for NYHOPS (**a**), HF radar (**b**), and drifter (**c**). Vector plots for the difference between near-surface current of drifter and NYHOPS (**d**) or HF radar (**e**) are also shown here. The time series of the wind speed from NDBC Buoy 44017 is shown in subplot (**f**). The time period for this analysis is from March 11, 2010 to March 25, 2010

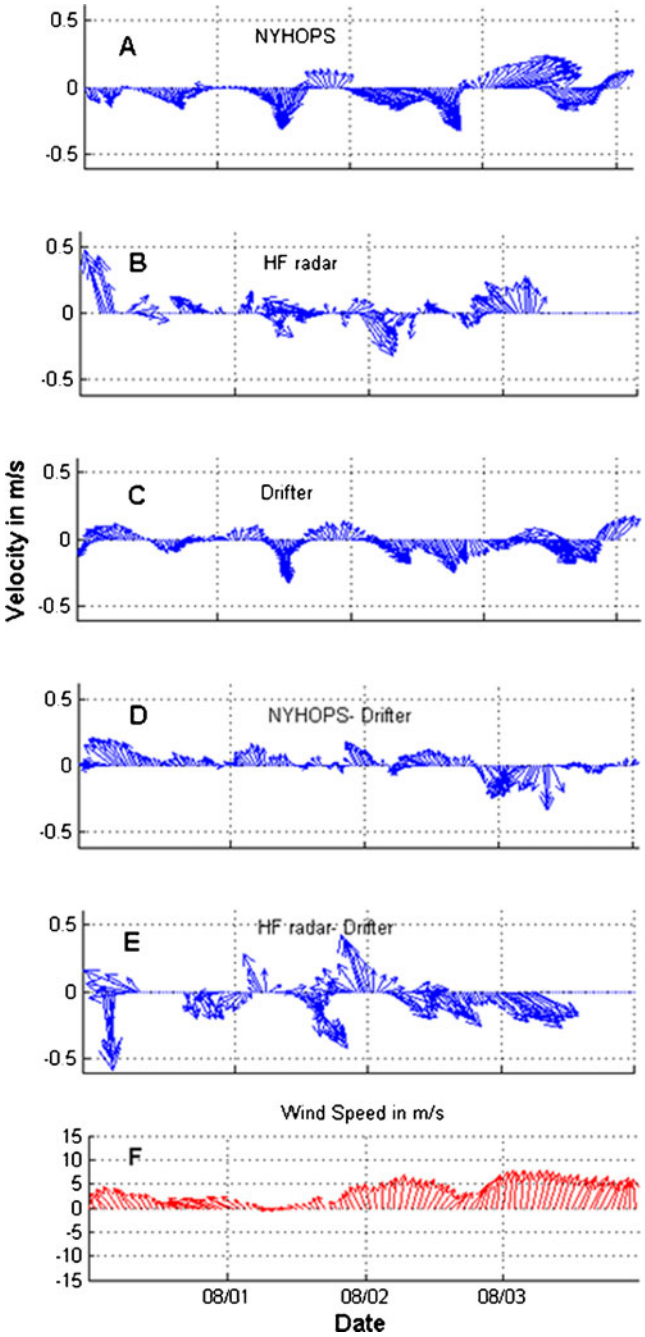

Fig. 5 Same as Fig. 4 but for track 2. The wind data are from NDBC Buoy 44065. The time period for this analysis is from July 31, 2010 to August 4, 2010

difference is relatively smaller when the wind is much weaker, especially seen during March 17 to 20. The inertial oscillations shown in the drifter track between March 20 and March 25 are well reproduced by NYHOPS and less well in the HF radar signal. The RMS differences of the NYHOPS and HF radar surface current vs. the drifter are both on the order of 10 cm s^{-1} (Table 3). This statistic holds for both the east–west (u) and north–south (v) velocity components. Although the magnitude of the mean current was underpredicted by almost 50 % by both NYHOPS and HF radar [vector mean current differences (MVVD) of 5 to 6 cm s^{-1} for a 11-cm-s^{-1} mean current], the general westward direction of the mean current observed by the drifter was correctly reproduced by both technologies (Table 2). NYHOPS did better with regard to mean vector direction in all three paths. The differences of mean vector direction between NYHOPS and drifters 1, 2, and 3 are 9°, 10°, and 3°, respectively. However, the differences of mean vector direction between HF radar and drifters 1, 2, and 3 are higher, with their values of 25°, 169°, and 18°, respectively.

The region where drifter 2 was deployed, the entrance to the NY/NJ Estuary, was clearly not a region where the HF radar current was able to derive the currents correctly as shown in the time series of Fig. 5 (Gopalakrishnan 2011). This drifter was a short deployment of 4 days. The observed inertial oscillations were nicely reproduced in the NYHOPS currents for the entire period. The RMS error between the NYHOPS and the drifter currents was approximately 10 cm s^{-1}, while the HF radar's RMS errors were about double that, with errors sometimes exceeding 50 cm s^{-1}. The NYHOPS vector mean currents were within 4 cm s^{-1} of the drifter observations.

The third track, covering 11 days in the fall of 2010, was located in the deeper waters on the southeast portion of the shelf. The time series shown in Fig. 6 suggest that both the NYHOPS and HF radar currents have periods when they agree well with the drifter currents and periods when they do not. The period between October 15 and 18, with surface winds over 10 m s^{-1} (Fig. 6), is captured by both the NYHOPS and HF radar currents. The mean vector velocity error was less than 1 cm s^{-1} for NYHOPS, while it was approximately equal to 9 cm s^{-1} for the HF radar currents. In general, the computed drifter currents are larger than the two other sets of currents, especially during October 20 to 22 (Fig. 6). During the period October 20 to 22, there is considerable error in both the model and HF radar currents when compared to the drifter-based currents. Based on available reanalysis from larger meteorological and hydrodynamic models that include the deeper ocean, it is hypothesized that the NYHOPS model results were degraded because the shelf break upwelling that existed at that time was not simulated in the model. The NYHOPS model shelf break forcing utilizes monthly temperature and salinity climatology and thus not able to simulate dynamic events originating in waters deeper than the shelf break. The shelf break upwelling event, coincident with frontal winds just offshore of the shelf break in the southern MAB, appears to have intensified the generally southwestward flowing current in the deeper area west of the Hudson canyon where the drifter was. Unrelated to this, the HF radar currents were in error because the coverage for track 3 at locations traveled

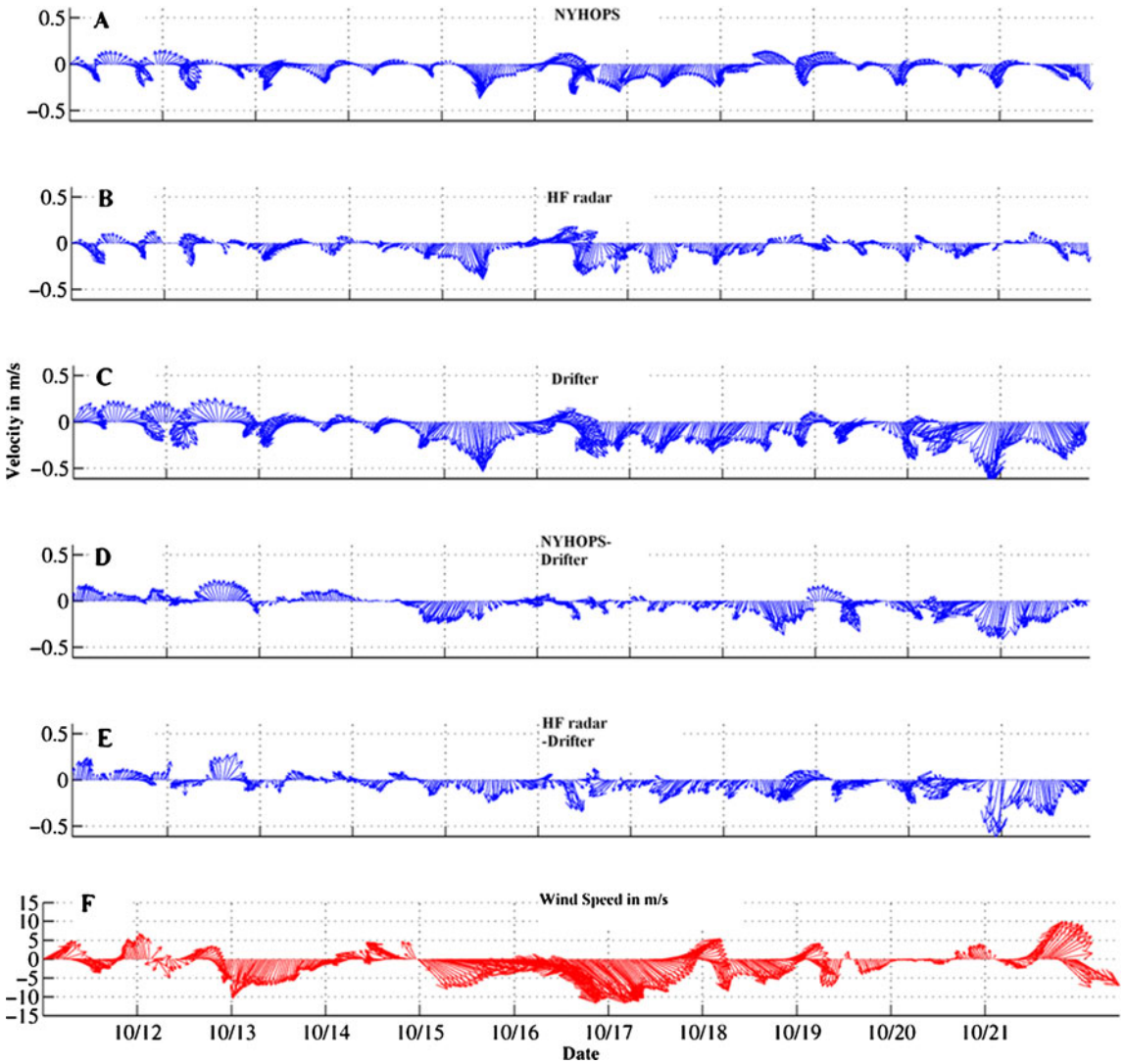

Fig. 6 Same as Fig. 4 but for track 3. The wind data are from NDBC Buoy 44066. The time period for this analysis is from October 11, 2010 to October 22, 2010

during October 20 to 22 is relatively low (see the coverage map of HF radar total currents, Fig. 1, insert). This low coverage of the HF radar signal will lead to less accurate surface currents (Lentz 2008a). Considering the average currents, it is apparent that the drifter currents were larger than both the NYHOPS and, especially, HF radar-derived currents.

Overall, RMS errors against the drifter currents were found to be on the order of 10 cm s^{-1} for both *u* and *v*. Mean HF radar currents appear to be generally lower than the ones observed by the drifters. The skill of the HF radar was similar during this period as to that found by Ullman et al. (2006). The RMS errors against the drifter currents when

Table 2 Mean velocity of east–west ($\overline{u}$) and north–south ($\overline{v}$) near-surface current from drifters, NYHOPS, and HF radar and the mean speed of their mean vector velocity difference (MVVD, as described in the text) for the three drifter tracks in 2010

Track no.	$\overline{u}$ (cm s^{-1})			$\overline{v}$ (cm s^{-1})			MVVD (cm s^{-1})	
	Drifter	NYHOPS	HF radar	Drifter	NYHOPS	HF radar	N–D	H–D
1	−9.9	−5.9	−4.2	−3.9	−1.3	−4.4	4.8	5.7
2	5.9	9.8	−2.9	−6.2	−7.0	2.0	4.0	12.0
3	−5.3	−4.6	−0.3	−14.9	−15.3	−7.2	0.8	9.2

N–D NYHOPS vs. drifter MVVD, *H–D* HF radar vs. drifter MVVD

Table 3 Root mean square difference (RMSD) of sea-surface currents ([*u*, (E–W)] and [*v*, (N–S)] component) between NYHOPS, HF radar, and drifters along the three drifter tracks in 2010

Track no.	RMSD of *u* (cm s^{-1})			RMSD of *v* (cm s^{-1})		
	N–D	H–D	N–H	N–D	H–D	N–H
1	12.1	10.3	10.4	8.6	9.1	10.6
2	8.5	18.8	22.0	10.4	18.5	17.9
3	11.1	13.3	9.7	13.7	14.5	8.7

N–D NYHOPS and drifter RMSD, *H–D* HF radar and drifter RMSD, *N–H* NYHOPS and HF radar RMSD

the wind speed is larger than 5 m s^{-1} were also analyzed and were found on the order of 10 cm s^{-1} for both NYHOPS and HF radar. The analysis suggests that NYHOPS and HF radar have similar skill in estimating the currents over the NJ shelf.

3.3 Particle tracking results analysis

The spaghetti diagram of the observed and GNOME-estimated trajectory for the whole deployment life of drifter 3 (Fig. 7, insert) shows that the trajectories computed using NYHOPS and HF radar currents reproduce the trajectory of the drifter for most of its lifetime. Both the simulated tracks using NYHOPS and HF radar currents yield shorter travel distances compared to the observed drifter path. In this case, the HF radar currents produce the shortest distance traveled. It should be pointed out that the mean velocity of HF radar at the time of drifter 3 is the lowest compared with NYHOPS and the drifter itself (Table 3). Also the MVVD between HF radar and drifter is the biggest for drifter 3. It was also shown in Fig. 6 that both NYHOPS and HF radar currents are weaker than the drifters along its path. In other words, the simulated drifter (represented as particles in GNOME) tends to travel slower than the real drifter. After October 17, 2010, the drifter entered an area where the surface current RMSD contours in Fig. 3 revealed relatively larger differences between NYHOPS and HF radar. This can also explain the difference between the simulated tracks from NYHOPS and HF radar currents in the southern part of the NYHOPS domain.

The ensemble mean separation distances and corresponding upper 95 % confidence intervals from the reseeding GNOME runs are shown in Fig. 7. Ensemble mean separation generally increases with time in a linear fashion. There is some indication that separations increase at a faster rate during the first day of the release, a finding consistent with Ullman et al. (2006). It does not appear that the separation distance is dominated by high frequency time or short spatial scale wavelengths. This suggests that both the NYHOPS and HF radar currents are representing tidal and inertial time scales correctly. The growing separation distance is dominated by errors in the mean flow causing the numerical drifters to slowly diverge from their observed position.

From the separation distance analysis (Fig. 7), NYHOPS performed slightly better in predicting the drifter location

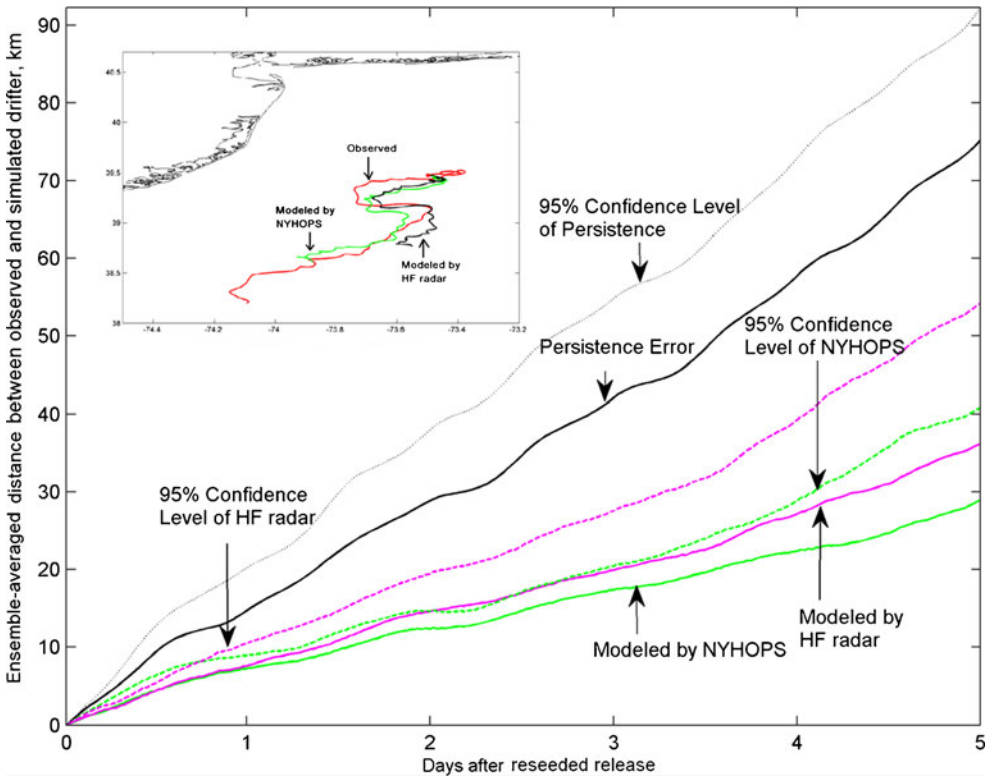

Fig. 7 Ensemble-averaged persistence error (*black solid line*) and separation distance between drifter 3 and numerical drifters based on NYHOPS (*green solid line*) and HF radar (*pink solid line*) surface currents as simulated with GNOME; 95 % upper confidence levels for the persistence error (*dotted black line*) and the separation distance of NYHOPS (*pink dash line*) and HF radar (*green dash line*) are also shown, from the "reseeding" experiments described in the text. *Insert* shows the observed drifter 3 trajectory (*red*) and the respective drifter trajectories simulated using surface currents from NYHOPS (*green*) and HF radar (*black*) over that drifter's complete deployment record

than the HF radar in this case. The separation distance for both HF radar and NYHOPS is less than 30 km in 5 days. Persistence is obviously not a good method of predicting the trajectory of a drifter subject to a general circulation current, so its separation over the 5 days grows to almost 70 km. Castellari et al. (2009) showed observation model drifter errors of 35–65 km over 10 days in the Adriatic Sea with a mean flow of around 2–20 cm s^{-1}. The work of Fan et al. (2004) reproduced drifter paths with position error of 30–80 km in a 10-day period in the Gulf of Mexico with mean surface velocities ranging from 10 to 40 cm s^{-1}. The mean surface current along track 3 is 25 cm s^{-1}.

4 Discussion and conclusions

In the present study, surface currents predicted by the NYHOPS hydrodynamic model, estimated by HF radar retrievals, and observed by drifters are compared. Harmonic analysis of NYHOPS and HF radar surface currents shows similar M_2 tidal ellipse parameters in the MAB, with differences of 2.4 cm s^{-1} in semi-major and 1.4 cm s^{-1} in semi-minor and 3° in orientation and 10° in phase. The comparison of tidal ellipses from NYHOPS and HF radar against observations shows that both NYHOPS and HF radar perform well and have similar skill in tidal current estimation. The presented analysis revealed that, in the open waters of the MAB, differences between HF radar and NYHOPS are mostly due to non-tidal effects, including meteorological forcing and buoyant plumes, which appear to be true.

NYHOPS and HF radar have a RMSD of 15 cm s^{-1} in the majority of the Middle Atlantic Bight. Differences are largest in the regions with strong surface currents, which include the New York Harbor area of the Hudson River plume, New Jersey coast, Delaware Bay, Long Island Sound, and the northern portion of the MAB shelf near Cape Cod. Away from coastal influences, in the open shelf water of the MAB, the presented RMSD analysis of non-tidal currents reveals that the biggest contributor to the apparent differences in the total current from the two technologies is due to inconsistent representation of the non-tidal effects. The normalized RMSD for the E–W and N–S current component against maximal tidal currents both have a value of about 20 % for the majority of the MAB. The variations in the depth of current estimations by the two technologies may contribute to those apparent differences and require further investigation.

From the current vector plot comparisons, both NYHOPS and HF radar appear generally reasonable in predicting the transient surface currents derived from the drifters along their trajectory. Both technologies have similar skill for the whole period, with RMS errors on the order of 10 cm s^{-1}. The HF radar currents were not accurate for drifter 2 which was in shallower waters adjacent to the NY Harbor mouth. Apparently, the HF radar's radial coverage was relatively low which often yields erroneous currents using the standard least-square methods employed here. It appears that NYHOPS was slightly better in reproducing mean current vectors (magnitude and directions) in this investigation. But it also lacked dynamic offshore temperature and salinity boundary conditions that appear to be important to the transient currents near the shelf break.

Particle tracking studies also reveal that both NYHOPS and HF radar yield very similar predictions and their separation distance from the observed drifter track was within 30 km after 5 days. For the case shown, the skill of the HF radar network in predicting drifter locations was slightly worse than that of NYHOPS. The inclusion of horizontal diffusion in the particle tracking model improved the predictions, and sensitivity tests verified that the 100-m^2-s^{-1} value given in literature (Ullman et al. 2006) is reasonable for the MAB. Based on the time period investigated here, it is recommended that both the NYHOPS and HF radar surface currents can be used alternatively for search and rescue simulations in the MAB with duration less than about 5 days. Both technologies produced simulated trajectories with separation distance less than 30 km before 5 days.

From the results of the present study, we find that both HF radar and NYHOPS have similar skills in terms of their capability for estimating and predicting near-surface currents. Based on NOAA guidelines on operational model skill (NOAA 2003), an RMS difference value of 17 cm s^{-1} is considered acceptable for operational use. NYHOPS and HF radar performance depends on the capture of tidal currents and non-tidal currents. The two technologies perform better when tide is dominant and may perform less well (with mixed success) during events when non-tidal effects are more dominant. Additional comparisons like those provided in this study for other time periods are suggested, as more recent drifter data become available and the technologies mature further. Validations of the model and HF radar currents against current meter observations should also be conducted. Also, new methods of extracting information from drifters for improving or validating models are encouraged and needed.

Acknowledgments This paper is made possible with the help from Dr. Josh Kohut of Rutgers University who kindly provided the hourly HF radar surface currents and answered so many questions we had. Thanks also to Dr. Arthur Allen of the US Coastal Guard and to Dr. Eoin Howlett of Applied Science of Associates for providing the SLMDB drifter data. We also thank Ms. Caitlin O' Connor of NOAA for providing technical advice with the GNOME software. This work was supported by NOAA, under Grant: NA11NOS0120038, "Phased Deployment and Operation of Mid-Atlantic Regional Coastal Observing System (MARCOOS)" administered through Rutgers University.

References

Barrick DE, Evans MW, Weber BL (1977) Ocean surface currents mapped by radar. Science 198:138–144

Beardsley RC, Boicourt WC (1981) On estuarine and continental-shelf circulation in the Middle Atlantic Bight. In: Warren BA, Wunsch C (eds) Evolution of physical oceanography. MIT, Cambridge, pp 198–233

Beegle-Krause CJ (2001) General NOAA Oil Modeling Environment (GNOME): a new spill trajectory model. IOSC 2001 Proceedings, 2:865–871

Bhushan S, Blumberg AF, Georgas N (2009) Comparison of NYHOPS hydrodynamic model SST predictions with satellite observations in the Hudson River tidal, estuarine, and coastal plume region. 11th International Conference in Estuarine and Coastal Modeling (ECM11). Spalding, M. L., Ph.D., P.E., American Society of Civil Engineers, Washington, pp 11–26

Blumberg AF, Galperin B (1990) On the summer circulation in New York Bight and contiguous estuarine waters. In: Cheng RT (ed) Residual currents and long-term transport, vol 38. Springer, New York, pp 451–468

Dzwonkowski B (2009) Surface current analysis of shelf water in the Central Mid-Atlantic Bight. University of Delaware, Delaware

Bruno M, Blumberg A, Herrington T (2006) The urban ocean observatory—coastal ocean observations and forecasting in the New York Bight. J Mar Sci Environ C4:1–9

Castellari S, Griffa A, Ozgokmen TM, Poulain PM (2009) Prediction of particle trajectories in the Adriatic Sea using Lagrangian data assimilation. J Mar Syst 29:33–50

Chang GC, Dickey TD, Schofield OM, Weidemann AD, Boss E, Pegau WS, Moline MA, Glenn SM (2002) Nearshore physical processes and bio-optical properties in the New York Bight. J Geophys Res 107(C9):3133–3149

Chant RJ, Glenn SM, Hunter E, Kohut J, Chen RF, Houghton RW, Bosch J, Schofield O (2008) Bulge formation of a buoyant river outflow. J Geophys Res 113:C01017. doi:10.1029/2007JC004100

Davis RE (1985) Drifter observations of coastal surface currents during CODE: the method and descriptive view. J Geophys Res 90:4741–4755

Di Liberto TE, Cole BA, Georgas N, Blumberg AF, Taylor AA (2011) Verification of multiple storm surge models and ensembles for the New York City metropolitan region. Weather Forecast 26:922–939

Dugan JP, Piotrowski CC (2003) Surface current measurement using visible image time series. Remote Sens Environ 1:309–319

Fan S, Oey LY, Hamilton P (2004) Assimilation of drifter and satellite data in a model of the Northeastern Gulf of Mexico. Cont Shelf Res 24:1001–1013

Fan SA, Blumberg AF, Bruno MS, Kruger D, Fullerton B (2006) The skill of an urban ocean forecast system. 9th International Conference in Estuarine and Coastal Modeling (ECM9). Spalding, M. L., Ph.D., P.E., American Society of Civil Engineers, South Carolina, pp 603–618

Flagg CN (1977) The kinematics and dynamics of the New England continental shelf and shelf/slope. Ph.D. thesis, MIT-WHOI Joint Program in Oceanography, Massachusetts

Frantantoni DM (2001) North Atlantic surface circulation during the 1990s' observed with satellite-tracked drifters. J Geophys Res 106 (C10):22067–22093

Gay PS, O'Donnell J, Edwards CA (2004) Exchange between Long Island Sound and adjacent waters. J Geophys Res 109:C06017. doi:10.1029/2004JC002319

Georgas, N. (2010) Establishing confidence in marine forecast systems: the design of a high fidelity marine forecast model for the NY/NJ harbor estuary and its adjoining waters. Dissertation, Stevens Institute of Technology

Georgas N (2012) Large seasonal modulation due to ice cover friction in a mid-latitude estuary. J Phys Oceanogr 42:352–369

Georgas N, AF Blumberg (2008) The New York Bight Shelf–Harbor dynamic study: ocean forecast sensitivity to forecasts of atmospheric forcing. Office of Naval Research, Arlington, 50 pp

Georgas N, Blumberg AF, Bruno MS, Runnels DS (2009) Marine forecasting for the New york urban waters and harbor approaches: the design and automation of NYHOPS. 3rd International Conference on Experiments / Process / System Modelling / Simulation & Optimization. Demos T. Tsahalis, Ph.D., University of Patras, Greece, 1:345–352 July 11 2009

Georgas N, Blumberg AF (2010) Establishing confidence in marine forecast systems: the design and skill assessment of the New York Harbor Observation and Prediction System, version 3 (NYHOPS v3). 11th International Conference in Estuarine and Coastal Modeling (ECM11). Spalding, M. L., Ph.D., P.E., American Society of Civil Engineers, Washington, pp 660–685

Georgas N, Blumberg AF, Herrington TO (2007) An operational coastal wave forecasting model for New Jersey and Long Island Waters. Reinhard E. Flick, Ph.D. Shore & Beach. American Shore and Beach Preservation Association. 75(2):30-35

Gopalakrishnan G, Blumberg AF (2012) Sensitivity of first-order Doppler region settings in the HF radar. Journal of Oceanography. J Oper Oceanogr. 5(1):75–87

Gong D, Kohut JT, Glenn SM (2010) Seasonal climatology of wind-driven circulation on the New Jersey Shelf. J Geophys Res 115: C4

Graber HC, Haus BK, Shay LK, Chapman RD (1997) HF radar comparisons with moored estimates of current speed and direction: expected differences and implications. J Geophys Res 102:18,749–18,766

Grant WD, Madsen OS (1979) Combined wave and current interactions with a rough bottom. J Geophys Res 84:1797–1808

Gurgel KW, Dzvonkovskaya A, Pohlmann T, Schlick T, Gill E (2011) Simulation and detection of tsunami signatures in ocean surface currents measured by HF radar. Ocean Dynamics. Springer Berlin, Heidelberg, pp 1–13

Kohut JT, Roarty HJ, Glenn SM (2006) Characterizing observed environmental variability with HF Doppler radar surface current mappers and acoustic Doppler current profilers: environmental variability in the coastal ocean. IEEE J Ocean Eng 31 (4):876–884

Lentz SJ (2008a) Observations and a model of the mean circulation over the Middle Atlantic Bight continental shelf. J Phys Oceanogr 38:1203–1221

Lentz SJ (2008b) Seasonal variations in the circulation over the Middle Atlantic Bight continental shelf. J Phys Oceanogr 38:1486–1500

Lipa B, Barrick D (1983) Least-squares methods for the extraction of surface currents from CODAR crossed-loop data: application at ARSLOE. IEEE J Ocean Eng 8(4):226–253

Lipa B, Nyden B, Barrick D, Kohut J (2008) HF radar sea-echo from shallow water. Sensors 8:4582–4599. doi:10.3390/s8084582

Moody JA, Butman B, Beardsley RC, Brown WS, Daifuku P, Irish JD, Mayer DA, Mofield HO, Petrie B, Ramp S, Smith P, Wright WR (1984) Atlas of tidal elevation and current observations on the northeast American continental shelf and slope. US Geol Surv Bull 1611:122

U.S. National Academies (2010) Pathways to urban sustainability: research and development on urban systems—summary of a workshop. The National Academies Press, Washington

NOAA (2003) NOS standard for evaluating operational nowcast and forecast hydrodynamic model systems. http://www.nauticalcharts.noaa.gov/csdl/docs/RD_standards_Hess_etal.pdf

Noble M, Butman B, Williams E (1983) On the longshelf structure and dynamics of subtidal currents on the Eastern United States continental shelf. J Phys Oceanogr 13:2125–2147

North EW, King DM et al (2010) Linking optimization and ecological models in a decision support tool for oyster restoration and management. Ecol Appl 20(3):851–866

Paduan JD, Graber HC (1997) Introduction to high-frequency radar: reality and myth. Oceanography 10(2):36–39

Paduan JD, Rosenfeld LK (1996) Remotely sensed surface currents in Monterey Bay from shore-based HF radar (CODAR). J Geophys Res 101(C9):20,669–20,686

Parks AB, Shay LK et al (2009) HF radar observations of small-scale surface current variability in the Straits of Florida. J Geophys Res 114:C08002. doi:10.1029/2008JC005025

Poulain PM (2001) Adriatic Sea surface circulation as derived from drifter data between 1990 and 1999. J Mar Syst 29:3–32

Pawlowicz R, Beardsley R, Lentz S (2002) Classical tidal harmonic analysis including error estimates in MATLAB using T_TIDE. Comput & Geosci 28:929–937

Rasmussen LL, Gawarkiewicz G, Owens WB (2005) Slope water, gulf stream, and seasonal influences on the southern Mid-Atlantic Bight circulation during the fall–winter transition. J Geophys Res 110. doi:10.1029/2004JC002311

Roarty H, Glenn S, Kohut J, Gong D et al (2010) Operation and application of a regional HF radar network in the Mid-Atlantic Bight. Mar Technol Soc 44(6):185–195

Rudnick DL, Davis RE, Eriksen CC, Fratantoni DM, Perry M (2004) Underwater gliders for ocean research. Mar Technol Soc J 38(1):48–59

Samelson RM, Allen JS, Mac Cready P (2008) Progress in coastal ocean modeling during CoOP. Oceanography 21(4):136–147

Schulz WJ, Mied RP, Snow CM (2012) Continental shelf wave propagation in the Mid-Atlantic Bight: a general dispersion relation. J Phys Oceanogr 42:558–568

Ullman DS, O'Donnell J, Kohut J, Fake T, Allen A (2006) Trajectory prediction using HF radar surface currents: Monte Carlo simulations of prediction uncertainties. J Geophys Res 111:C12005. doi:10.1029/2006JC003715

Xu FH, Oey LY (2011) The origin of along-shelf pressure gradient in the Middle Atlantic Bight. J Phys Oceanogr 41(9):1720–1740. doi:10.1175/2011JPO4589.1